Synthesis and Characterization of Nanocomposite Films with a Titania Glass Matrix by the Sol–gel Route

T. K. Kundu and D. Chakravorty*†

[1]Indian Association for the Cultivation of Science, Jadavpur, Calcutta: 700 032, India
[2]Also affiliated to Jawaharlal Nehru Centre for Advanced Scientific Research, Bangalore: 560 064, India

Films of thickness ∼3 μm containing nanosized metal particles of iron, nickel and copper respectively were grown on a Corning glass slide using a sol-gel technique. The particle sizes had values in the range 6.8 to 20.1 nm. Optical absorption characteristics of different specimens were studied over the wavelength range 230 to 830 nm. An absorption maximum was observed at wavelength varying from 270 to 300 nm depending on the nanocomposite system. The data were analysed on the basis of effective medium theories viz., Maxwell-Garnett (MG) and Bruggemann (BR) models respectively. MG model showed better agreement with experimental results than BR theory. The volume fraction as estimated from the least square fitting procedure was found to be in the range 2 to 3%. Copyright © 1999 John Wiley & Sons, Ltd.

Keywords: thin films; nanocomposites; iron; nickel; copper; titania glass; optical absorption characteristics

1. INTRODUCTION

The Sol-gel technique has emerged as a powerful route to the synthesis of a wide range of materials.[1] High purity and homogeneity can be attained by this method which has the advantage of a low temperature processing requirement.[2,3] A number of composites containing nanometre-sized metals dispersed in a silica glass matrix have been prepared using this method.[4,5] These have been used to investigate the behaviour of materials in their nanocrystalline state.[6–8] As part of a wider investigation we have explored the possibility of making nanocomposites with a titania (TiO_2) glass matrix. TiO_2 cannot be made in the glassy form by the conventional melt–quench route. In the present work we have synthesized by the sol–gel method the nanocomposites containing iron, nickel and copper respectively dispersed in a TiO_2-based glass matrix in thick-film form. Optical absorption characteristics of these films have been studied and the details are reported in this paper.

2. EXPERIMENTAL

A mixture of 120 cm^3 of ethyl alcohol and 30 cm^3 of acetic acid was stirred for 0.5 h. After adding 18 cm^3 of tetraisopropyl orthotitanate had been added to this mixture, it was stirred for 1 h, the divided into three equal parts (denoted by A_1, A_2 and A_3 respectively). Three mixtures (B_1, B_2 and B_3) were then prepared:
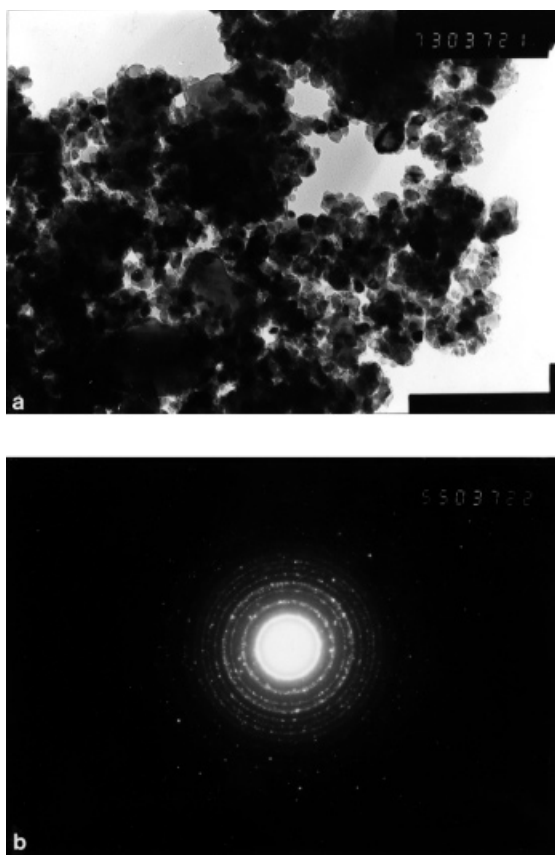
(B_1) 1 g ferric chloride + 10 cm^3 ethyl alcohol + 10 cm^3 distilled water
(B_2) 2 g nickel chloride + 10 cm^3 ethyl alcohol + 10 cm^3 distilled water
(B_3) 2 g cupric chloride + 10 cm^3 ethyl alcohol + 10 cm^3 distilled water

These are denoted by B_1, B_2 and B_3 respectively. Finally three sols were prepared by mixing A_1 and B_1, A_2 and B_2, A_3 and B_3 respectively.

Films were prepared by dipping chemically cleaned Corning glass slides (dimensions 3 cm × 1 cm × 0.1 cm into the solutions prepared as

* Correspondence to: D. Chakravorty, Indian Association for the Cultivation of Science, Jadavpur, Calcutta 700 032, India.
E-mail: mls@iacs.ernet.in
†Also affiliated to Jawaharlal Nehru Centre for Advanced Scientific Research, Bangalore: 560 064, India.

Figure 1 (a) Transmission electron micrograph of specimen containing iron and reduced at 675 °C for 20 min; (b) electron diffraction pattern of the same specimen.

described above. The films were initially dried at room temperature, then oven dried at 100°C for 24 h, heated slowly to 300°C and kept for 1 h. Finally they were subjected to reduction treatment in hydrogen at temperatures in the range 550 to 675°C for 10–20 minutes to precipitate nanosized metal particles within the gel-derived glass matrix. The thicknesses of the films were measured by an SF 220 surface profiler supplied by Planer Products Ltd., U.K. The films were found to have thicknesses in the range 3 to 4 μm.

For microstructural studies gel pieces having compositions identical to those described as above and subjected to the same reduction treatment were finely ground in an agate mortar. The resulting powders were dispersed in acetone kept in a test tube which was then placed in an ultrasonic bath for about 0.5 h. A drop of this dispersion was then deposited on a carbon coated copper grid which was dried in air and subsequently mounted in the sample

Table 1. Comparison of interplanar spacings d_{hkl} nm obtained from electron diffraction data with ASTM values for Fe/TiO$_2$ specimen reduced at 675 °C for 20 min

Observed	ASTM	
	Fe	TiO$_2$
0.271		0.252
0.219		0.218
0.202	0.2026	0.205
0.178		
0.1587		0.1624
0.148		0.148
0.141	0.143	0.145
0.123		0.120

chamber of a JEM 200 CX transmission electron microscope.

The optical absorption characteristics of the nanocomposite films were determined by taking the spectra in a Hitachi 300 Spectrophotometer over the wavelength range 230 to 830 nm. The absorption coefficient was calculated from equation [1]:

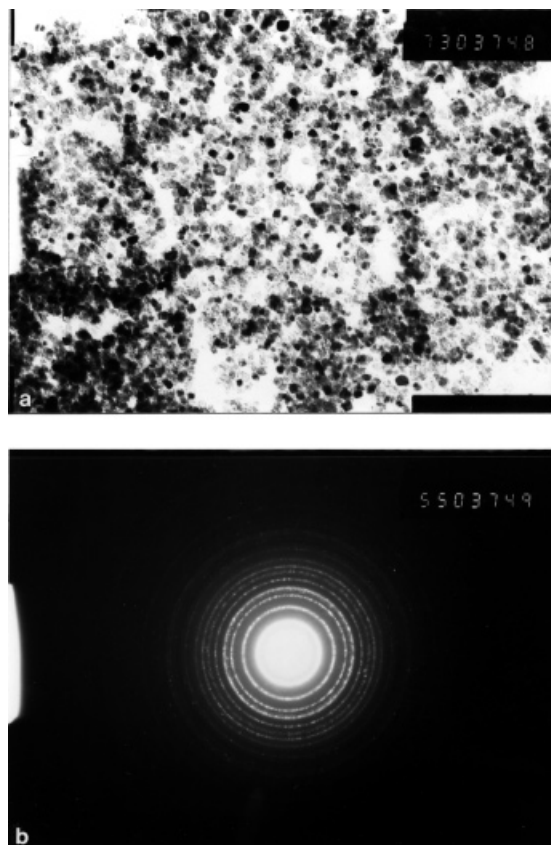$$\alpha = \frac{1}{t}\ln\left(\frac{1}{T}\right) \qquad (1)$$

where T is the transmittance of the sample and t its thickness.
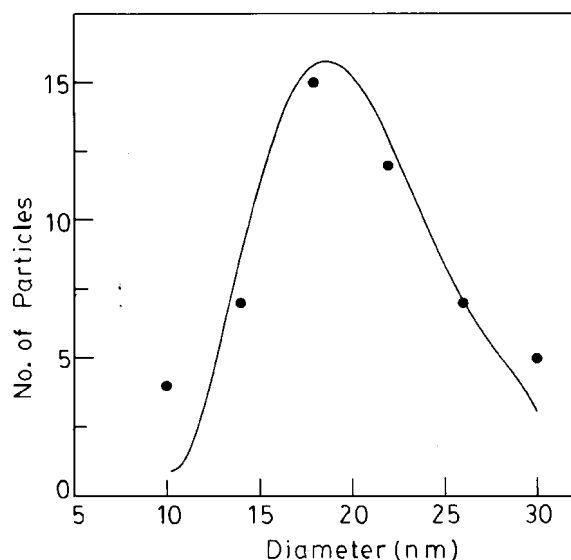
Figure 2 Particle size distribution of the specimen shown in Fig. 1: ●, experimental; —, theoretical.
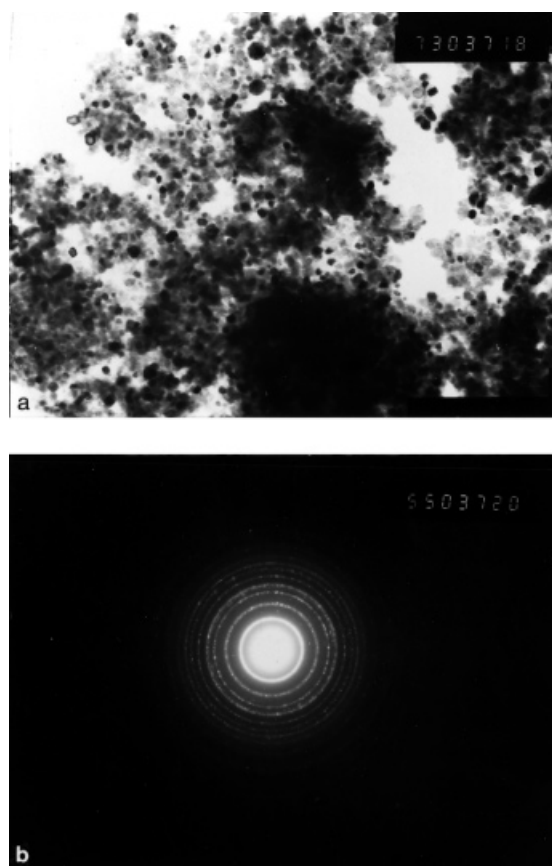
Figure 3 (a) Transmission electron micrograph of specimen containing nickel and reduced at 660 °C for 10 min; (b) electron diffraction pattern of the same specimen.

Figure 4 (a) Transmission electron micrograph of specimen containing copper and reduced at 660 °C for 10 min; (b) electron diffraction pattern of the same specimen.

3.   RESULTS AND DISCUSSION

Figure 1(a) shows the transmission electron micrograph for a specimen containing iron which was reduced at 675°C for 20 minutes. Figure 1(b) is the electron diffraction pattern. Interplanar spacing (d_{hkl}) values have been calculated from the diameters of the rings and are summarised in Table 1. Standard d_{hkl} values for metallic iron as well as titania are also listed in the table. It is evident from the observed values that both iron and titania particles are present in this sample. The microstructure shows a distribution of particles having diameters in the range 10 to 30 nm. The data have been fitted to a log normal distribution function given by equation [2].

$$\Delta n = \frac{1}{\sqrt{2\pi}\ln\sigma}\exp\{-[ln(\frac{x}{\bar{x}})/\ln\sigma]\}\Delta(\ln x) \quad [2]$$

where Δn is the fractional number of particles per logarithmic diameter interval $\Delta(\ln x)$, $\bar{x}$ is the median diameter and σ the geometric standard deviation. The particle size distribution is shown in Fig. 2, in which the points represent the experimental data and the solid line the least-squares fitted curve using Equation [2]. The extracted values of $\bar{x}$ and σ are shown in Table 4 (below). The microstructure and the electron diffraction rings as shown in Fig. 1 are typical of all other samples containing Fe and TiO_2 particles.

The electron micrograph and electron diffraction pattern of a specimen containing nickel and subjected to a reduction treatment at 660 °C for 10 min are shown in Figs 3(a) and 3(b) respectively. Figures 4(a) and 4(b) show the micrograph and electron diffraction pattern for a specimen containing copper which was subjected to a reduction treatment at 660 °C for 10 min. These are typical of
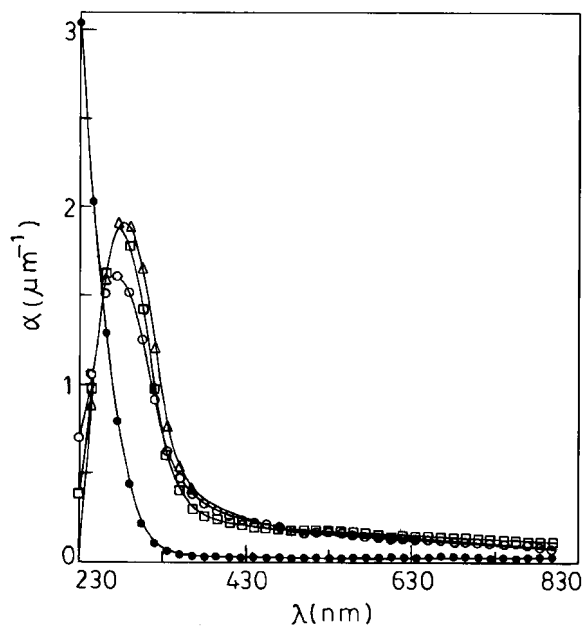
Table 2. Comparison of d_{hkl} nm obtained from electron diffraction data with ASTM values for Ni/TiO$_2$ specimen reduced at 660 °C for 10 min

| | ASTM | |
Observed	Ni	TiO$_2$
0.271		0.252
0.219		0.218
0.202	0.2034	0.205
0.178	0.1762	
0.1587		0.1624
0.148		0.148
0.141		0.145
0.123	0.1246	0.120

Table 3. Comparison of d_{hkl} nm obtained from electron diffraction data with ASTM values for Cu/TiO$_2$ specimen: reduced at 660 °C for 10 min

| | ASTM | |
Observed	Cu	TiO$_2$
0.271		0.252
0.219		0.218
0.208	0.2088	0.205
0.202		
0.178	0.180	
0.1587		0.1624
0.148		0.148
0.141		0.145
0.123	0.1278	0.120

Figure 5 Variation of optical absorption coefficient as a function of wavelength for nanocomposite specimens in the Fe/TiO$_2$ series: ●, specimen without metal; ○, specimen no. 1; □, specimen no. 2; △, specimen no. 3.

all specimens in these two series. Tables 2 and 3 show the calculated values of d_{hkl} as obtained from Figs 3(b) and 4(b) respectively. Comparison with ASTM values shows the presence of TiO$_2$ particles also in the specimens containing either nickel or copper. The histograms of particle sizes for all specimens were analysed using Equation [2] as described earlier. Table 4 summarizes the values of mean diameter x and geometric standard deviation as extracted by this analysis for all the specimens studied here. It is evident from these results that the particle size of the different metallic species can be increased by raising the reduction temperature and

Table 4. Summary of heat treatment schedule, median diameter and geometric standard deviation for particles in different specimens

Specimen no.	Nanocomposite system	Reduction treatment in hydrogen		Median diameter x (nm)	Geometric standard deviation σ (nm)
		Temp (°C)	Duration (min)		
1	Fe/TiO$_2$	550	10	12.0	1.4
2	Fe/TiO$_2$	660	10	14.3	1.6
3	Fe/TiO$_2$	675	20	20.1	2.3
4	Ni/TiO$_2$	550	10	12.2	1.3
5	Ni/TiO$_2$	660	10	15.7	1.2
6	Ni/TiO$_2$	675	20	18.3	1.4
7	Cu/TiO$_2$	550	10	6.8	1.8
8	Cu/TiO$_2$	660	10	13.1	1.9
9	Cu/TiO$_2$	675	20	18.4	2.1
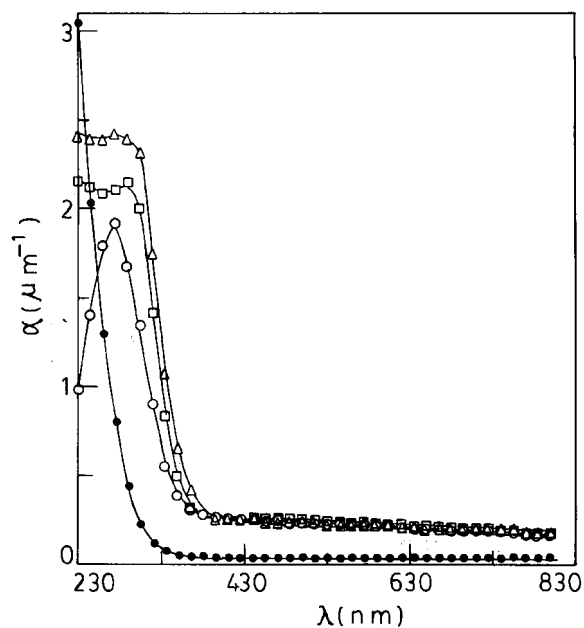
Figure 6 Variation of optical absorption coefficient as a function of wavelength for nanocomposite specimens in the Ni/TiO$_2$ series: ●, specimen without metal; ○, specimen no. 4; □, specimen no. 5; △, specimen no. 6.
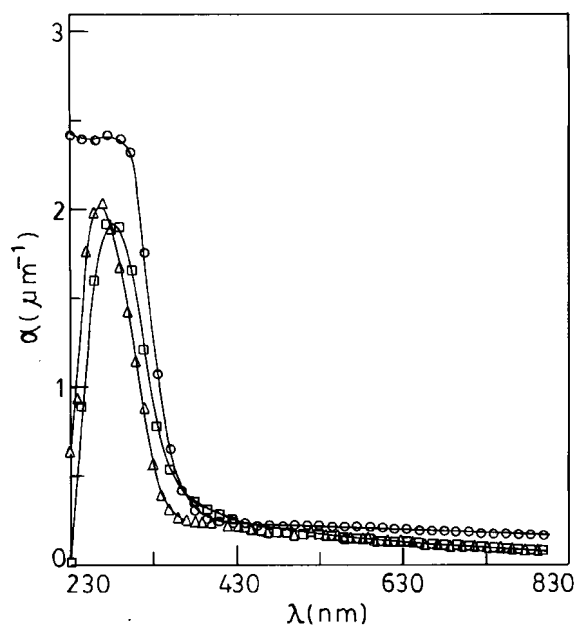
Figure 8 Comparison of optical absorption for nanocomposites containing different metallic species of comparable particle size: □, specimen no. 3; ○, specimen no. 6; △, specimen no. 9.
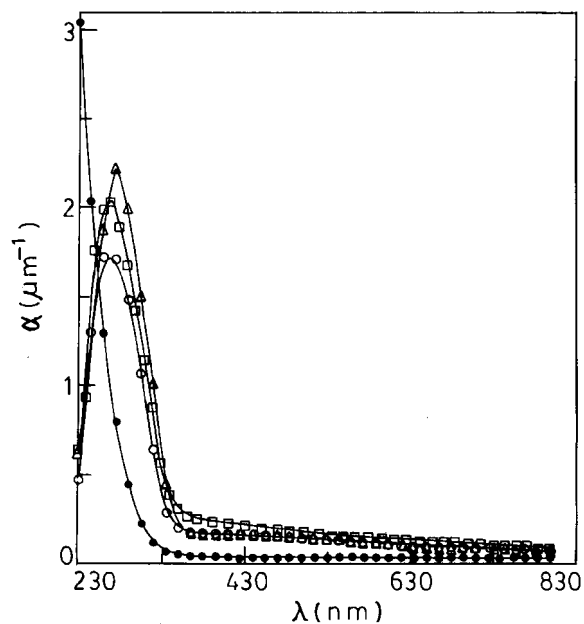
Figure 7 Variation of optical absorption coefficient as a function of wavelength for nanocomposite specimens in the Cu/TiO$_2$ series: ●, specimen without metal; ○, specimen no. 7; □, specimen no. 8; △, specimen no. 9.

duration of treatment. The particle sizes obtained in the present series of samples range from 6.8 to 18.4 nm. Such an increase is consistent with the diffusion-controlled growth of the metallic phases.

Figure 5 shows the variation of absorption coefficient as a function of wavelength (λ) for specimens (1,2 and 3) containing nanoparticles of iron. The curves show an absorption maximum at around 280 nm. The maximum is seen to shift to higher wavelength as the metal particle size is increased. Figures 6 and 7 show the α versus λ plots for different specimens in the Ni/TiO$_2$ and Cu/TiO$_2$ series respectively. In the former case the maximum is around 300 nm, in the latter case it is found to be around 270 nm. The results are similar to these described in Fig. 5. The absorption mechanism responsible for the behaviour is discussed below. Figure 8 compares the absorption characteristics for nanocomposites containing different metallic phases but having comparable particle diameters. It is evident that the nickel glass composites give the highest absorption whereas those containing copper and iron have absorption values similar to each other. Although no apparent

reason could be adduced for this behaviour, the following discussion and the results obtained by fitting the data to the equations governing effective medium theories suggest that this arises simply because of a higher volume fraction of the metallic phase.

The present series of specimens comprise composites containing nanoparticles of different metallic species dispersed within a glass medium. These are therefore ideal systems for their optical behaviour to be analysed by different effective medium theories developed earlier. We have used Maxwell–Garnett[9] and Bruggeman[10] models respectively in the present study.

In the Maxwell–Garnett (MG) model the particles in the medium are assumed to be spherical, having identical diameters and separated from each other so that they scatter light independently. Then the expression for the effective medium dielectric permittivity ε^{MG} in this model is given by Equation [3]:

$$\frac{\bar{\varepsilon}^{MG} - \varepsilon_m}{\bar{\varepsilon}^{MG} + 2\varepsilon_m} = f\frac{\varepsilon - \varepsilon_m}{\varepsilon + 2\varepsilon_m} \qquad [3]$$

where ε_m is the dielectric permittivity of the matrix phase, f is the volume fraction or filling factor of the metal phase in the composite and ε is the permittivity of individual metal particles.

The Bruggemann (BR) model is based upon the assumption that the particles are embedded in an effective medium in such a way that the average single-site scattering is zero. The effective dielectric permittivity ε^{BR} according to this model is given by Equation [4]:

$$\bar{\varepsilon}^{BR} = \varepsilon_m \frac{1 - f + \frac{1}{3}\sum_j f_j\beta_j}{1 - f - \frac{2}{3}\sum_j f_j\beta_j} \qquad [4]$$

where f_j is the filling factor of particles with diameters d_j such that

$$\sum_j f_j = f \qquad [5]$$

where f is the filling factor of the metal phase,

$$\beta_j = \frac{1}{3}\sum_{l=1}^{3} \frac{\varepsilon_j - \varepsilon}{\bar{\varepsilon} + L_l(\varepsilon_j - \bar{\varepsilon}^{BR})} \qquad [6]$$

where ε_j is the size-dependent dielectric permittivity of particles with diameters d_j and L_l are their depolarization factors.

The size-dependent dielectric permittivity of each of the metallic phases has been calculated

Table 5. Values of ω_{pb}, τ_b and V_{Fb} used for calculation of dielectric permittivities for different metallic species

Metallic phase	ω_{pb} $(10^{15}$ rad s$^{-1})$	τ_b $(10^{-15}$ s$)$	V_{Fb} $(10^6$ m s$^{-1})$
Iron	6.1	2.1	2.0
Nickel	6.5	1.9	2.0
Copper	4.5	2.0	1.6

from the corresponding bulk data using the Equation [7]:[12]

$$\varepsilon_j(\omega) = \varepsilon_{expt}(\omega) - \varepsilon_{expt}^{Drude}(\omega) + \varepsilon_j^{Drude}(\omega) \qquad [7]$$

where ω is the angular frequency of the radiation concerned,

$$\varepsilon_{expt}^{Drude}(\omega) = 1 - \omega^2_{pb}/\omega(\omega + i/\tau_b) \qquad [8]$$

$$\varepsilon_j^{Drude}(\omega) = 1 - \omega^2_{pd_j}/\omega(\omega - i/\tau_b) \qquad [9]$$

where ω_{pb} and τ_b are the bulk plasma frequency and mean electron lifetime respectively, ω_{pd_j} represents the apparent plasma frequency of particle d_j, and τ_j is given by

$$\tau_j^{-1} = \tau_b^{-1} + 2V_{Fb}/d_j \qquad [10]$$

where V_{Fb} is the bulk Fermi velocity of electrons. In the present case we assume $\omega_{pd_j} \approx \omega_{pb}$.[12] We have estimated the values of ω_{pb} for different metals from the corresponding dielectric permittivity data as a function of frequency,[13] and τ_b and V_{Fb} have been calculated using the free-electron model.[14] Table 5 summarizes the values of ω_{pb}, τ_b and V_{Fb} for different metallic species used in our calculation. A value of $\varepsilon_m = 17$ has been assumed based on dielectric measurements carried out on gel-derived TiO$_2$ films before any reduction treatment was given. The size-dependent filling factors f_j in equations [4] and [5] are estimated from Equation [11]:
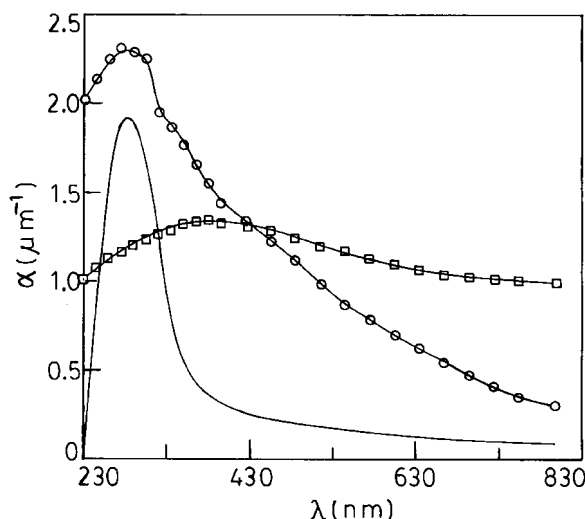
$$f_j = \omega_j f \qquad [11]$$

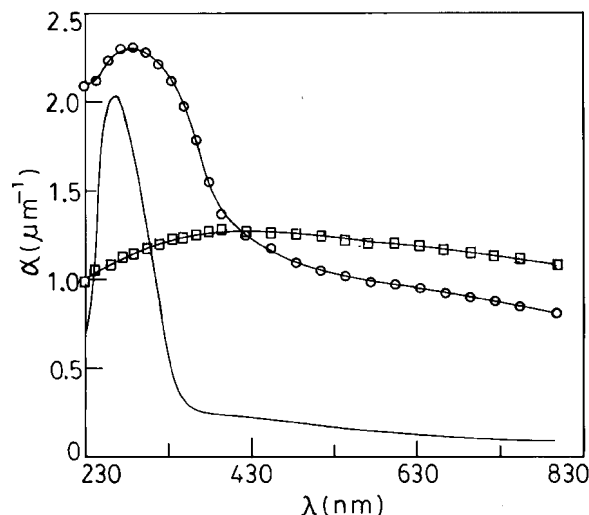where ω_j is the weight factor and is given by

$$\omega_j = d_j^3 n_j / \sum d_j^3 n_j \qquad [12]$$

n_j being the number of particles with diameter d_j.

The optical absorption coefficient α was calcu-

Figure 9 Comparison of experimental with theoretical curves obtained from the MG and BR models for specimen no. 3: —, experimental; ○, MG model; □, BR model.

lated using Equation [13]

$$\alpha(\omega) = \left(\frac{\omega}{c}\right)\left(\frac{\bar{\varepsilon}_2}{\bar{\varepsilon}_1^{1/2}}\right) \qquad [13]$$

The experimental data for different specimens were least-squares fitted to theoretical expressions as given above for the two models using f as a

Figure 10 Comparison of experimental with theoretical curves obtained from the MG and BR models for specimen no. 5; —, experimental; ○, MG model; □, BR model.
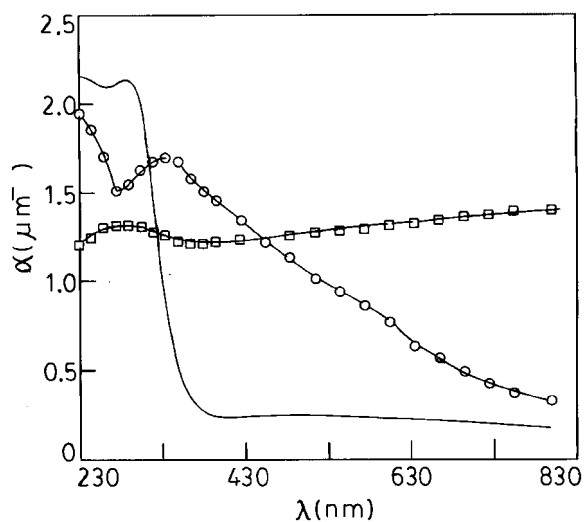
Figure 11 Comparison of experimental with theoretical curves obtained from the MG and BR models for specimen no. 9: —, experimental; ○ the MG model; □, the BR model.

parameter. The value of f could not be estimated from the micrographs because the thicknesses of the samples used for electron microscopy were not known accurately. Figures 9, 10 and 11 show comparisons of experimental results with the theoretical curves for typical specimens in the Fe/TiO$_2$, Ni/TiO$_2$ and Cu/TiO$_2$ series respectively. It is evident from these Figures that the Maxwell–Garnett model gives better qualitative agreement with experiments. This implies that ultrafine metal particles are well separated from each other, thereby satisfying the assumptions made in the Maxwell–Garnett model. The filling factors f as

Table 6. Values of filling factors *f* for different specimens as estimated by the effective medium theories

Specimen no.	Composite	Filling factor f (vol%)	
		MG model	BR model
1	Fe/TiO$_2$	1.7	1.2
2	Fe/TiO$_2$	2.3	1.5
3	Fe/TiO$_2$	2.9	2.0
4	Ni/TiO$_2$	1.9	0.8
5	Ni/TiO$_2$	2.7	1.8
6	Ni/TiO$_2$	3.4	2.0
7	Cu/TiO$_2$	2.2	1.9
8	Cu/TiO$_2$	2.6	2.2
9	Cu/TiO$_2$	3.1	2.0

estimated by this fitting procedure are summarized in table 6 for the different specimens. The *f* values estimated from the MG theory are found to be higher than those calculated from the BR model. It was shown earlier that BR model works better in the case of systems containing clusters of nano-particles.[12] Evidently the BR model does not represent adequately the morphological character-istics of the present set of specimens.

In summary, nanocomposite films of thickness ~3 μm containing iron, nickel and copper respec-tively in a TiO_2 glass matrix were synthesized using a sol–gel technique. The particle sizes were in the range 6.8–20.1 nm, depending on the reduction treatment given to the samples. Detailed optical absorption spectra in the wavelength range 230–830 nm were recorded. An absorption maximum was observed around 280 nm in all the specimens. Maxwell–Garnett and Bruggemann models were used to fit the absorption characteristics. The MG theory gives a better qualitative agreement with the experimental results.

REFERENCES

1. R. Roy, *Science* **238**, 1664 (1987).
2. L. L. Hench, and M. J. R. Wilson, *J. Non-Cryst Solids* **121**, 234 (1990).
3. R. Reisfeld, D. Brusilovsky, M. Eyal, E. Miron, Z. Burshstein, and J. Ivri, *Chem. Phys. Lett.* **160**, 43 (1989).
4. A. Chatterjee, D. Das, D. Chakravorty, and K. Choudhury, *Appl. Phys. Lett.* **57**, 1360 (1990).
5. A. Chatterjee, A. Datta, A. K. Giri, D. Das, and D. Chakravorty, *J. Appl. Phys.* **72**, 3832 (1992).
6. S. Roy, A. Chatterjee, and D. Chakravorty, *J. Mater. Res.* **8**, 689 (1993).
7. S. Roy, D. Das, D. Chakravorty, and D. C. Agarwal, *J. Appl. Phys.* **74**, 4749 (1993).
8. T. K. Kundu, and D. Chakravorty, *J. Mater. Res.* **11**, 200 (1996).
9. J. C. Maxwell-Garnett, *Phil. Trans. R. Soc.* **203**, 385 (1904).
10. D. A. G. Bruggemann, *Ann. Phys. (Leipzig)* **24**, 636 (1935).
11. A. Kawabata, and R. Kubo, *J. Phys. Soc. Jpn.* **21**, 1765 (1966).
12. C. G. Granqvist, and O. Hunderi, *Phys. Rev.* **16**(8), 3513 (1977).
13. P. B. Johnson, and R. W. Christy, *Phys. Rev.* **B9**, 5056 (1974).
14. C. Kittel, *Introduction to Solid State Physics*, New York Wiley, 1974.